

Abundances in eight bulge stars from the optical and near-infrared

Patrícia da Silva^{1,2}, B. Barbuy², H. Erandes³, S. O. Souza², J. G. Fernández-Trincado⁴, and D. González-Díaz⁴ *

¹ Observatoire de Paris, LERMA, Collège de France, CNRS, PSL University, Sorbonne University, 75014, Paris – e-mail: patricia2.silva@alumni.usp.br

² Instituto de Astronomia, Geofísica e Ciências Atmosféricas, Departamento de Astronomia, Universidade de São Paulo, 05508-090, SP, Brazil

³ Lund Observatory, Department of Astronomy and Theoretical Physics, Lund University, Box 43, SE-221 00 Lund, Sweden

⁴ Instituto de Astronomía, Universidad Católica del Norte, Av. Angamos 0610, Antofagasta, Chile

Received, accepted

ABSTRACT

Context. The abundances of the α -elements are key for understanding the early chemical enrichment of the Galactic bulge. The elements of interest present lines in different wavelength regions, and some of them show lines only in part of the spectra. In the present work, the CNO trio, the α -elements Mg, Si, Ca, and Ti, and odd-Z Na and Al are examined as measured from optical and H -band lines.

Aims. The aim of this work is to carry out a detailed comparison of stellar parameters and abundances derived in the optical and near-infrared (H -band). We also inspect the best available lines for a list of bulge stars previously analyzed by the Apache Point Observatory Galactic Evolution Experiment (APOGEE) team in the H -band and by our group in the optical. This work is mainly of interest to spectroscopists.

Methods. In the present work, we compared the stellar parameters and abundance results derived from APOGEE H -band spectra with optical analyses based on Ultraviolet and Visual Echelle Spectrograph at the Very Large Telescope (VLT/UVES) data for eight bulge stars.

Results. We point out the most suitable wavelength region for each of the studied elements, and highlight difficulties in the derivation of stellar parameters both in the optical and H -band. The near-infrared will allow observations of a large number of stars in the near future given new instruments soon to be available. The identification of spectral lines in this spectral region and the investigation of their reliability are ongoing efforts worldwide. New instruments will also allow simultaneous observation of H -band and optical.

Key words. Galaxy: bulge – Stars: abundances – (Galaxy:) globular clusters: individual: NGC 6522, NGC 6558, HP 1, Palomar 6

1. Introduction

Abundances in the Galactic bulge are being scrutinized for a better definition of the fast star formation rate and identification of the supernovae that enriched the medium very early on (e.g., Barbuy et al. 2018a; Matteucci 2021). This applies to field and globular cluster stars, with the latter also involving new progress in our understanding of self-enrichment and the multiple stellar populations that undoubtedly occurred in almost all clusters (Pitto et al. 2015; Renzini et al. 2015; Milone et al. 2017; Bastian & Lardo 2018; Milone & Marino 2022).

The light elements are discriminators of the type of supernova and nucleosynthesis that formed them, and in order to use them, reliable abundance values are needed. Consequently, in this work, we investigate the possible differences between the abundance derivation from the optical and the near-infrared (NIR) for eight stars analyzed in the optical by our group and also available from NIR spectra.

Instrumentation in astronomy allowing observations in the NIR has progressed significantly in the recent past. Apache Point Observatory Galactic Evolution Experiment (APOGEE–Majewski et al. 2017) allows high-resolution spectroscopy in

the H -band at a resolution of $R \sim 22\,000$ carried out at the 2.5m Sloan Foundation Telescope at the Apache Point Observatory in New Mexico (APOGEE-1 and APOGEE-2N: Beaton et al. 2021), and the 2.5m du Pont Telescope at Las Campanas Observatory in Chile (APOGEE-2S). Spectroscopy in the JHK bands will be intensified with the James Webb Space Telescope (JWST), and new spectrographs on ground-based telescopes such as the Multi-Object Optical and Near-IR Spectrograph (MOONS) at the Very Large Telescope (VLT), the Warm Infrared Echelle spectrograph to REalize Decent high-resolution spectroscopy (WINERED) at the Magellan telescope (see Minniti et al. (2024)), and the Multi-Object Spectrograph for Astrophysics, Intergalactic-medium studies and Cosmology (MOSAIC) at the Extremely Large Telescope (ELT) at the European Southern Observatory (ESO), among others.

The aim of the present work is to compare available lines and results that can be obtained in the optical and H -band for a list of elements. This study is useful as it indicates the most reliable lines in the optical and/or H -band—which is of particular interest for observations with the ELT/MOSAIC that should allow simultaneous observations in the NIR and selected regions in the optical at resolutions of 6,000 and 20,000 (Hammer et al. 2021).

The analysis of H -band spectra in the APOGEE project is carried out through a Nelder-Mead algorithm (Nelder & Mead 1965), which simultaneously fits the stellar parameters effective temperature (T_{eff} , gravity ($\log g$), metallicity ($[Fe/H]$), and mi-

* Observations collected at the European Southern Observatory, Paranal, Chile (ESO), under programmes 65.L-0340A, 93.D-0123A 97.D-0175A, 0103.D-0828A, 71.B-517 and 73.B-0074; and APOGEE project.

cro-turbulence velocity (v_t), together with the abundances of carbon, nitrogen, and alpha-elements with the APOGEE Stellar Parameter and Chemical Abundances Pipeline - ASPCAP pipeline, which is based on the FERRE code (García-Pérez et al. 2016). Spectroscopists within the APOGEE community are carrying out continuous and intensive work, but improvements are still needed for some elements and lines.

Jönsson et al. (2018) carried out an important verification of the accuracy of the ASPCAP results, and reported previous analyses with the same intent: Hawkins et al. (2016) used the DR12 APOGEE to analyze stars with asteroseismic analysis from Kepler light curves, and found differences regarding Si, S, Ti, and V. Souto et al. (2016) used the DR13 APOGEE to analyze spectra of 12 giant stars belonging to the open cluster NGC 2420 ($[\text{Fe}/\text{H}] \sim -0.16$), and found differences in the abundances of Na, Al, and V. Fernández-Trincado et al. (2016) manually reanalyzed the DR12 APOGEE spectrum of one peculiar metal-poor field giant star with a globular cluster second-generation abundance pattern, and found differences in the abundances of C, N, O, Mg, and Al of about 0.3 dex.

Holtzman et al. (2018) described the series of technical steps of the ASPCAP procedure, and the grids of synthetic spectra used to derive stellar parameters. Jönsson et al. (2018) carried out a comparison between results from DR13 and DR14, as well as selected literature results, with mean differences reported in their Table 5. Jönsson et al. (2020) and Hayes et al. (2022) studied the details of several lines from DR16 and DR17 results, and pointed out problems and limitations.

In Razera et al. (2022), our group analyzed 58 moderately metal-poor bulge field stars ($-2.0 < [\text{Fe}/\text{H}] < -0.8$) from APOGEE spectra, and identified the most suitable spectral lines for deriving the abundances of C, N, O, Mg, Si, Ca, and Ce given that some of the ASPCAP adopted lines are too faint in these metal-poor stars. These authors confirmed the Mg, Si, and Ca from ASPCAP, whereas O and Ce were found to be more abundant than the ASPCAP values.

In the present work, we identified eight stars previously analyzed by our group from optical high-resolution spectra collected with the Ultraviolet and Visual Echelle Spectrograph (UVES) at the VLT. Importantly, these sources were also observed with APOGEE. For this sample, we carried out a detailed comparison of stellar parameters and abundance results and inspected the available lines for a list of elements.

In Section 2, we list the sample stars and report previous calculations. In Section 3, we describe the present calculations. In Section 4 we compare the stellar parameters and abundances derived from the optical and near-infrared, and show how we carried out fits to lines both in the optical and in the near-infrared. We discuss our results in Section 5 and draw conclusions in Section 6.

2. The sample

The sample consists of eight stars analyzed in the optical using the UVES spectrograph at the VLT (ESO), and for which there are available observations with APOGEE. These stars are from the following globular clusters: one star from HP 1 (Barbuy et al. 2016), two stars from NGC 6558 (Barbuy et al. 2018a), one star from NGC 6522 (Barbuy et al. 2014), and one star from Palomar 6 (Souza et al. 2021). In Ernandes et al. (2018) the abundances of Sc, V, Mn, Cu, and Zn were derived for most of these stars. The sample is completed with three bulge field stars analyzed for different elements, namely C, N, and O in Zoccali et al. (2006); Lecœur et al. (2007); Jönsson et al. (2017), and Friaça

& Barbuy (2017) (the latter is adopted), Mn and Zn in Barbuy et al. (2013, 2015) and da Silveira et al. (2018), and Co and Cu in Ernandes et al. (2020).

The H -band data are from the APOGEE project, which is part of the Sloan Digital Sky Survey III and IV (SDSS; Blanton et al. 2017). The project aimed to investigate Milky Way stars observed at high resolution and high signal-to-noise ratios (S/Ns) in the H -band. The project SDSS-IV technical summary, the SDSS telescope, and APOGEE spectrograph are described in Blanton et al. (2017); Gunn et al. (2006); Wilson et al. (2019), respectively, whereas Zasowski et al. (2013, 2017); Beaton et al. (2021); Santana et al. (2021) describe the APOGEE and APOGEE-2 target selections. The data release 17 (DR17) contains high-resolution ($R \sim 22,500$) H -band spectra (15140–16940 Å) for about 7×10^5 stars. The 2.5m Sloan Foundation Telescope in New Mexico, USA, and the 2.5m Irene du Pont Telescope in Las Campanas Observatory in Chile were used, covering the northern and southern skies respectively. In the present work, we reanalyze the optical spectra for the elements Na, Mg, Al, Si, Ca, and Ti, and in the H -band the elements C, N, O, Mg, Al, Si, and Ca for the lines reported in Table 1.

2.1. Previous calculations

In the optical, we analyzed UVES spectra observed in the range 4800–6800 Å based on synthetic spectra calculations carried out with the code PFANT described in Barbuy et al. (2018b)¹. This code is an update of the original FANTOM or ABON2 Meudon code by M. Spite. Each model atmosphere was interpolated in the MARCS grids (Gustafsson et al. 2008).

In the H -band, the ASPCAP in its last release, DR17, issued stellar parameters obtained from a spectroscopic solution that minimizes the errors in seven dimensions (T_{eff} , $\log g$, $[\text{Fe}/\text{H}]$, v_t , $[\alpha/\text{Fe}]$, $[\text{C}/\text{Fe}]$, $[\text{N}/\text{Fe}]$), and yields the abundances of several elements. For DR17, the results were obtained with new spectral grids constructed using the Synspec (Hubeny & Lanz 2017; Hubeny et al. 2021) spectral synthesis code that incorporates NLTE level populations for Na, Mg, K, and Ca (Osorio et al. 2020).

2.2. Previous results

In Table 2 we report the identification of the stars, their coordinates, and colours. Table 3 provides the stellar parameters derived in the optical and using the APOGEE ASPCAP procedure together with respective references.

Table 4 lists the abundances derived for the sample stars in the APOGEE DR17 release. These data correspond to the spectroscopic or so-called noncalibrated APOGEE abundances adopted in this paper for comparison reasons. These elemental abundances were obtained in the table (allStar-dr17-synspec_rev1.fits)² in the APOGEE site.

Table 5 gives the abundances obtained with UVES for each sample star from Barbuy et al. (2013, 2014, 2015, 2016, 2018a); Ernandes et al. (2018, 2020); Friaça & Barbuy (2017); Lecœur et al. (2007); Souza et al. (2021) and van der Swaelmen et al. (2016).

¹ The code is available at <http://trevisanj.github.io/PFANT>.

² https://www.sdss4.org/dr17/irspec/spectro_data/

Species	λ (Å)	χ_{ex} (eV)	log gf Smith13	log gf (VALD3)	log gf (NIST)
Mg I	15740.716	5.931	-0.262	-0.323	-0.212
	15748.988	5.932	0.276	0.049	-0.338
	15765.842	5.933	0.504	0.320	-0.337
	15879.521	5.946	-1.248	-2.102	-1.998
	15886.261	5.946	-1.555	-1.742	-1.521
Al I	16718.957	4.085	0.290	0.152	0.220
	16750.539	4.088	—	0.408	—
	16763.359	4.087	-0.524	-0.550	-0.480
Si I	15376.831	6.222	-0.649	-0.701	—
	15960.063	5.984	0.107	0.130	0.197
	16060.009	5.954	-0.566	-0.452	-0.429
	16094.787	5.964	-0.168	-0.088	-0.078
	16215.670	5.964	-0.665	-0.565	-0.575
	16680.770	5.984	-0.140	-0.138	-0.090
Ca I	16828.159	5.984	-1.102	-1.058	-1.012
	16150.763	4.532	-0.229	0.362	—
	16155.236	4.532	-0.619	-0.758	—
	16157.365	4.554	-0.208	-0.219	—
	16197.075	4.535	—	0.089	—
	16204.087	4.535	—	-0.627	—

Table 1. Lines studied in the H -band. Oscillator strengths, log gf, reported in Smith et al. (2013), Smith et al. (2021), or given in VALD3 or Kurucz (1993)³, and NIST are reported.

3. New calculations

We recomputed the abundances of C, N, O, Mg, Al, Si, and Ca in the H -band, and Na, Mg, Al, Si, Ca, and Ti in the optical using the code TURBOSPECTRUM from Alvarez & Plez (1998) and Plez (2012). Model atmosphere grids are from Gustafsson et al. (2008). The solar abundances are from Grevesse & Sauval (1998): $A(\text{C})=8.55$, $A(\text{N})=7.97$, from Steffen et al. (2015): $A(\text{O})=8.76$, and from Smith et al. (2021): $A(\text{Na})=6.17$, $A(\text{Mg})=7.53$, $A(\text{Al})=6.37$, $A(\text{Si})=7.51$, $A(\text{Ca})=6.31$, $A(\text{Ti})=4.90$.

Table 1 reports the lines in the H -band that we verified in the spectra of the eight sample stars. The atomic line list employed is that from the APOGEE collaboration, together with the molecular lines described in Smith et al. (2021). The lines of the studied elements C, N, O, Na, Al, Mg, Si, and Ca (Ti is excluded) were recently examined by Razera et al. (2022) and Barbúy et al. (2023).

In the optical, the lines measured are listed, for example, in Barbúy et al. (2016). For the calculations, we adopted the line list from VALD3 (Ryabchikova et al. 2015). The new VALD3 line list includes hyperfine structure when possible and needed. The molecular lines include CH from Masseron et al. (2014), CN from Brooke et al. (2014), C2 from Brooke et al. (2013), MgH from Skory et al. (2003), and TiO, including the α , β , γ , γ' , ϵ , δ (and ϕ in the NIR), from Jorgensen (1994).

Below we give a brief description of the methods employed in the analysis of optical and H -band spectra in order to make clear that there are differences between them due to the different lines available in each spectral region.

In the optical, initial parameters based on photometric indicators are adopted, and iteratively modified based on ionization and excitation equilibria of Fe I and Fe II lines of different ionization and excitation energies until the parameters converge.

³ 1995 Atomic Line Data (R.L. Kurucz and B. Bell) Kurucz CD-ROM No. 23. Cambridge, Mass.: Smithsonian Astrophysical Observatory.

The excitation equilibrium requires a constant Fe abundance for Fe I lines with different excitation energies χ_{exc} , and is affected mainly by iterating the value of the effective temperature. The ionization equilibrium requires similar Fe abundances from Fe I and Fe II lines, which are affected mainly by the gravity $\log g$ value. Finally, the microturbulence velocity v_t is obtained by imposing a constant Fe abundance versus equivalent width (EW) of Fe I lines.

In the H -band, the Fe I lines have almost all of their excitation energies in the range 5.5 to 7.0 eV, which means that the concept of excitation equilibrium cannot be used as initial temperature indicator. Therefore, initial indication for the effective temperature are photometric indices. The ASPCAP pipeline derives their noncalibrated stellar parameters, in this case from Data Release 17 (DR17), using a spectroscopic solution that minimizes the chi-squared differences between the observations and the models in the following seven dimensions: T_{eff} , $\log g$, $[\text{Fe}/\text{H}]$, v_t , $[\alpha/\text{Fe}]$, $[\text{C}/\text{Fe}]$, and $[\text{N}/\text{Fe}]$. As we demonstrate below, the fit to molecular lines of CN, CH, CO, and OH is a powerful tool for constraining stellar parameters, in particular the effective temperature.

In the following sections, we carry out abundance derivations using the two sets of stellar parameters—that is, those obtained with the APOGEE ASPCAP procedure and the detailed analyses with the optical spectra observed with UVES—that are reported in Table 3.

4. Stellar parameters

In this section, we compare effective temperature T_{eff} , gravity $\log g$, metallicity $[\text{Fe}/\text{H}]$, and microturbulence velocity v_t obtained from analyses of spectra in the optical and the H -band, and element abundances derived in both cases.

4.1. Comparison of stellar parameters from optical and near-infrared spectra

The comparison of stellar parameters obtained from detailed analysis in the optical and the derivation adopted with the ASPCAP software in the H -band can provide information as to the advantages and disadvantages of using each of these bands.

From Table 3, we make the following observations:

- For all stars, the microturbulence velocity is very low in the ASPCAP parameters.
- Stars N6522-402361, OGLE-82760, and OGLE-392918 have very close parameters derived in the optical and H -band.
- Star HP1-2 has very similar T_{eff} and $\log g$, but lower $[\text{Fe}/\text{H}]$ and v_t from H -band relative to optical.
- Stars NGC6558-283, NGC6558-1160, Palomar6-401, and OGLE-545277 have lower T_{eff} by about 300 K, higher $\log g$ by about 0.7dex, lower v_t by about 0.8 km.s^{-1} , and relatively similar metallicities for the metal-poor stars and lower $[\text{Fe}/\text{H}]$ by about 0.5dex for the metal-rich star OGLE-545277, that is, according to H -band relative to optical analyses.

A discussion on which are the best stellar parameters is deferred to the following sections involving comparisons of element abundances, that in turn also help us to discriminate the most likely results for each of the sample stars according to their stellar population group.

HP1									
ID internal	Gaia	2MASS	OGLE	α_{2000}	δ_{2000}	V	I	H	
HP1-2	4058638335451540352	2M17310585-2958354	—	17:31:05.852	-29:58:35.5	16.982	14.332	11.268	
NGC 6558									
ID internal	Gaia	2MASS	OGLE	α_{2000}	δ_{2000}	V	I	H	
283	4048864158119516416	2M18102223-3145435	—	18:10:22.228	-31:45:43.340	15.883	14.378	12.564	
1160	4048864432989873408	2M18101768-3145246	—	18:10:17.682	-31:45:24.570	15.586	14.063	12.000	
NGC 6522									
ID internal	Gaia	2MASS	OGLE	α_{2000}	δ_{2000}	V	I	H	
B-107	4050198110543819008	2M18033660-3002164	402361	18:03:36.59	-30:02:16.1	15.977	14.313	11.803	
Palomar 6									
ID internal	Gaia	2MASS	OGLE	α_{2000}	δ_{2000}	V	I	H	2MASS
401	4061102272286853888	2M17433806-2613426	—	17 43 38.05	-26 13 42.7	17.43	14.40	11.46	
Bulge Field									
ID internal	Gaia	2MASS	OGLE	α_{2000}	δ_{2000}	V	I	H	2MASS
BW-b4	4050186355212762624	2M18040535-3005529	545277	18 04 05.340	-30 05 52.50	16.95	14.42	11.803	
BW-b5	4050205119984310144	2M18041328-2958182	82760	18 04 13.270	-29 58 17.80	18.832	14.45	12.032	
BW-f6	4050196456967930240	2M18033691-3007047	392918	18 03 36.890	-30 07 04.30	18.387	14.272	12.043	

Table 2. Sample stars: Identifications from internal name, Gaia, 2MASS and OGLE numbers. Star NGC6522-402361 is also identified as B-107 in Barbuy et al. (2014), and stars OGLE-545277, - 82760 and -392918 are also identified as BW-b4, BW-b5 and BW-f6 in Lecureur et al. (2007).

ID	APOGEE						UVES					
	T_{eff} (K)	$\log g$	v_t (km s $^{-1}$)	[Fe/H]	Ref.	SNR	T_{eff} (K)	$\log g$	v_t (km s $^{-1}$)	[Fe/H]	Ref.	SNR
HP1-2	4565	1.54	0.42	-1.229 \pm 0.017	DR17	122	4630	1.70	1.60 –	-1.00	B06	70
N6558-283	4570	2.01	0.30	-1.043 \pm 0.021	DR17	46	4800	2.10	1.00 –	-1.20	B18	80
N6658-1160	4454	1.94	0.20	-1.178 \pm 0.019	DR17	80	4900	2.60	1.30 –	-1.15	B18	80
N6558-1160	4729	1.80	1.61	-1.15 \pm 0.008	DGD23	–	–	–	–	–	–	–
N6522-402361	4993	2.43	-0.11	-1.131 \pm 0.022	DR17	64	4990	2.00	1.40 –	-1.12	B14	110
N6522-402361	–	–	–	–	–	–	4990	2.10	1.40	-1.11	B09-G	–
N6522-402361	–	–	–	–	–	–	4950	2.00	1.40	-1.06	Z08-G	–
Pal6-401a	4294	1.62	0.24	-0.911 \pm 0.018	DR17	61	4500	1.50	1.0	-1.00	S21	50
Pal6-401b	4396	1.80	0.24	-0.911 \pm 0.018	DR17	105	–	–	–	–	–	–
OGLE-545277	3955	2.23	0.06	0.540 \pm 0.010	DR17	58	4300	1.40	1.4	0.07	L07	60
OGLE-545277	–	–	–	–	–	–	4100	1.84	1.2	0.35	Z08-G	–
OGLE-82760	3967	2.02	0.10	0.317 \pm 0.010	DR17	87	4000	1.60	1.2	0.17	L07	60
OGLE-82760	–	–	–	–	–	–	4300	1.87	1.5	0.25	Z08-G	–
OGLE-392918	4135	1.76	0.19	-0.260 \pm 0.013	DR17	69	4100	1.70	1.5	-0.21	L07	60
OGLE-392918	–	–	–	–	–	–	4600	1.97	1.4	0.05	Z08-G	–

Table 3. ASPCAP (noncalibrated) spectroscopic parameters for the stars from APOGEE, and from DGC23: (González-Díaz et al. 2023, hereafter DGD23) in the H -band, and spectroscopic parameters from UVES from B16: Barbuy et al. (2016), B18: Barbuy et al. (2018a), B14: Barbuy et al. (2014), S21: Souza et al. (2021), L07: Lecureur et al. (2007) in the optical. Parameters obtained from lower resolution FLAMES-GIRAFFE spectra from B09: Barbuy et al. (2009) and Z08: Zoccali et al. (2008), indicated by -G, are also reported.

4.2. CNO abundances from Turbospectrum

We first fitted the full region $\lambda\lambda$ 15525 - 15595 Å, which contains molecular lines of CO, OH, and CN, as described in Barbuy et al. (2021b) and Razera et al. (2022). The most important and clean of these features is the CO bandhead at $\lambda\lambda$ 15578 - 15579 Å, which is sensitive to the C abundance, recalling that the less abundant species is the one that controls the feature. After fitting this CO feature, we checked and fitted the OH lines at 15535.46, 15536.7, 15565.91, and 15568.78 Å by changing the O abundance. Finally, we inspected the CN features along this region of the spectrum, which provides preliminary information on the N abundance. Figure 1 shows the fit to this region for star OGLE-3932918 computed with the stellar parameters from the optical analysis. For verification and fine tuning, a few OH, CN, and CO

lines in other regions are fitted, as shown in Razera et al. (2022). Table 6 shows the CNO abundances from TURBOSPECTRUM calculations of APOGEE spectra for both sets (optical and H -band) of stellar parameters.

For NGC6558-283, NGC6558-1160, and Pal6-401, it appears that the effective temperatures deduced in the optical are too high (Barbuy et al. 2018c), and are incompatible with the strength of the molecular lines of CO and OH in particular. For NGC6558-1160, the ASPCAP effective temperature ($T_{eff} = 4454$ K) appears suitable, and those somewhat higher ones ($T_{eff} = 4729$ K) by González-Díaz et al. (2023) (DGD23) are acceptable. We note that DGD23 derived stellar parameters from VVV photometry, and these are closer to the ASPCAP-calibrated parameters ($T_{eff} = 4628.5$ K, $\log g = 1.813$, $v_t = 0.2145$ km.s $^{-1}$).

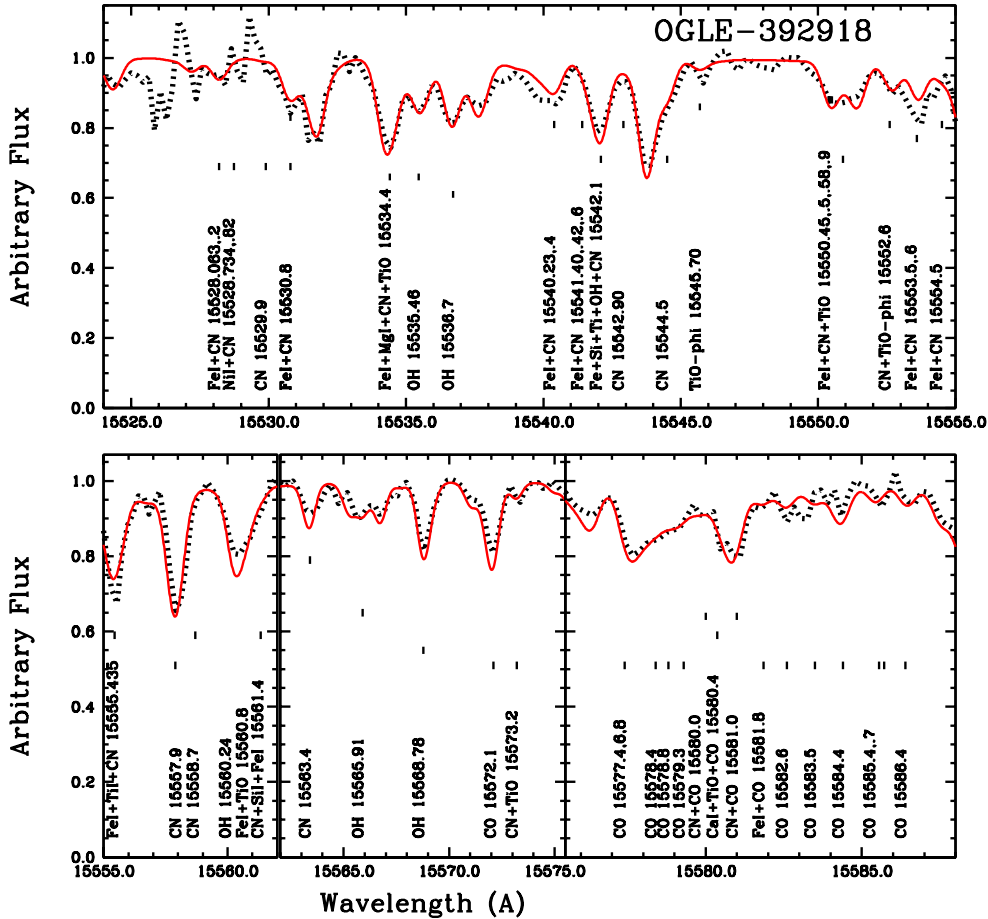


Fig. 1. OGLE-392918: APOGEE spectrum fitted in the region $\lambda\lambda$ 15525 - 15595 Å (black dotted lines) and synthetic spectra adopting the UVES stellar parameters (red lines).

We conclude that the stellar parameters obtained from ASPCAP, which correspond to a spectroscopic solution that minimizes the chi-squared differences between the observations and the models in seven dimensions (T_{eff} , $\log g$, $[\text{Fe}/\text{H}]$, v_t , $[\alpha/\text{Fe}]$, $[\text{C}/\text{Fe}]$, and $[\text{N}/\text{Fe}]$), lead to reliable parameters that are constrained by the strength of molecular lines. In the optical, Fe I of different excitation energies are used to constrain the effective temperature, together with Fe I and Fe II lines used to impose ionization equilibrium, and the goodness of the procedure depends on reliable equivalent widths of Fe II, which are often difficult to obtain, in particular given the blends and noise in the spectra of metal-poor stars.

The ASPCAP stellar parameters and CNO abundances are clearly more suitable in the case of NGC6568-1160, for which the APOGEE spectra have a good S/N, although this is not fully applicable to NGC6558-283 and NGC6522-402361, which have rather low S/N APOGEE spectra. We consider this to be an important point concerning the ASPCAP derivation of stellar parameters, as well as the C, N, and O abundances. In other words, the fit to molecular lines appears to be a very suitable technique for deriving reliable effective temperatures. For the optical, we assumed the same C, N, and O abundances derived from the H -band, which is more reliable for deriving C, N, and O given that,

in the optical, the C and N indicators—that is, the C_2 and CN bandheads—are very weak.

4.3. The atomic lines of the odd-Z Na, Al, and α -elements Mg, Ca, Si, and Ti

The sample stars are in the metallicity range $-1.1 \lesssim [\text{Fe}/\text{H}] \lesssim +0.3$. Below, we describe which region, that is, the H -band or optical, provides better indicators for each of the elements studied here.

Magnesium: Mg I lines are well-fit for all stars for the given abundances both from ASPCAP and UVES analyses. For more metal-poor stars, most of these lines will become faint, and in those cases the stronger lines, such as Mg I 5528 Å and the Mg I triplet at 5167-5183 Å, might be appropriate.

Silicon:

Clearly the Si I lines in the H -band are very suitable as Si abundance indicators; these comprise seven very good lines (we discard the Si I 15361.161 Å line, which is weak). In the optical, the lines are fainter for the metal-poor stars, but still good indicators, and very suitable for the metal-rich stars. The H -band Si I lines, which come from Smith et al. (2013, 2021), are shown in Figure 2 for the star NGC6522-402361. In this figure, the line observed Si I 16060.009 Å, appears broader than the com-

Element	HP1-2	283	1160	402361	401	545277	82760	392918
APOGEE								
C	-0.35 ± 0.04	-0.16 ± 0.05	-0.21 ± 0.04	0.45 ± 0.06	-0.14 ± 0.03	0.074 ± 0.005	0.087 ± 0.006	0.158 ± 0.013
	-0.55 ± 0.04	-0.25 ± 0.05	-0.27 ± 0.05	0.17 ± 0.07	-0.27 ± 0.04	0.070 ± 0.011	0.082 ± 0.011	0.151 ± 0.019
N	0.89 ± 0.05	0.81 ± 0.06	0.07 ± 0.06	0.39 ± 0.08	0.34 ± 0.04	0.326 ± 0.010	0.282 ± 0.011	0.220 ± 0.021
	1.02 ± 0.04	0.88 ± 0.05	0.16 ± 0.05	0.47 ± 0.06	0.47 ± 0.04	0.254 ± 0.013	0.258 ± 0.013	0.236 ± 0.022
O	0.26 ± 0.03	0.29 ± 0.05	0.34 ± 0.04	0.51 ± 0.07	0.32 ± 0.03	0.011 ± 0.009	0.038 ± 0.009	0.321 ± 0.016
	0.19 ± 0.04	0.23 ± 0.06	0.33 ± 0.05	0.60 ± 0.07	0.32 ± 0.04	-0.015 ± 0.012	0.029 ± 0.012	0.277 ± 0.019
Na	-0.23 ± 0.12	-0.31 ± 0.14	0.22 ± 0.13	-0.66 ± 0.16	0.16 ± 0.11	0.27 ± 0.03	0.15 ± 0.03	0.20 ± 0.06
	-1.24 ± 0.23	0.45 ± 0.29	0.05 ± 0.26	-0.87 ± 0.35	0.21 ± 0.21	0.33 ± 0.04	0.19 ± 0.04	0.23 ± 0.09
Mg	0.21 ± 0.03	0.24 ± 0.03	0.29 ± 0.03	0.25 ± 0.03	0.28 ± 0.03	-0.002 ± 0.013	0.059 ± 0.013	0.492 ± 0.018
	0.09 ± 0.03	0.20 ± 0.03	0.24 ± 0.03	-0.11 ± 0.03	0.23 ± 0.03	-0.035 ± 0.013	-0.025 ± 0.013	0.310 ± 0.019
Al	0.10 ± 0.03	0.28 ± 0.05	-0.05 ± 0.04	0.26 ± 0.05	0.08 ± 0.04	0.03 ± 0.03	0.06 ± 0.03	-0.14 ± 0.04
	0.27 ± 0.04	0.42 ± 0.05	0.13 ± 0.05	0.06 ± 0.05	0.29 ± 0.05	0.11 ± 0.04	0.10 ± 0.03	0.47 ± 0.04
Si	0.198 ± 0.022	0.15 ± 0.03	0.20 ± 0.03	0.39 ± 0.03	0.418 ± 0.024	-0.059 ± 0.012	-0.042 ± 0.012	0.279 ± 0.017
	0.23 ± 0.03	0.17 ± 0.04	0.24 ± 0.04	0.27 ± 0.04	0.42 ± 0.03	-0.017 ± 0.017	0.011 ± 0.017	0.228 ± 0.024
P	0.58 ± 0.15	-0.29 ± 0.20	-0.54 ± 0.17	-	0.56 ± 0.14	0.07 ± 0.05	0.10 ± 0.05	0.29 ± 0.08
S	0.51 ± 0.10	0.10 ± 0.13	0.24 ± 0.12	0.09 ± 0.13	0.75 ± 0.10	-0.07 ± 0.03	-0.05 ± 0.03	0.45 ± 0.06
	0.54 ± 0.13	0.37 ± 0.18	0.31 ± 0.16	0.09 ± 0.18	0.66 ± 0.15	-0.01 ± 0.04	-0.03 ± 0.04	0.35 ± 0.08
K	0.23 ± 0.09	-0.05 ± 0.13	0.28 ± 0.11	0.28 ± 0.12	0.14 ± 0.10	-0.15 ± 0.04	0.20 ± 0.04	0.07 ± 0.06
	0.14 ± 0.08	-0.03 ± 0.10	0.27 ± 0.09	0.38 ± 0.10	0.10 ± 0.09	-0.48 ± 0.04	0.10 ± 0.04	0.08 ± 0.06
Ca	0.14 ± 0.05	0.31 ± 0.06	0.28 ± 0.06	-0.37 ± 0.07	0.22 ± 0.05	-0.035 ± 0.010	-0.010 ± 0.011	0.145 ± 0.022
	0.10 ± 0.04	0.34 ± 0.05	0.27 ± 0.05	-0.19 ± 0.06	0.28 ± 0.04	-0.046 ± 0.016	-0.007 ± 0.016	0.15 ± 0.03
Ti	-0.01 ± 0.05	0.16 ± 0.07	-0.01 ± 0.06	0.31 ± 0.09	0.01 ± 0.05	-	-	-
	0.03 ± 0.05	0.22 ± 0.06	0.10 ± 0.05	0.29 ± 0.07	0.03 ± 0.05	0.730 ± 0.020	0.421 ± 0.020	0.09 ± 0.03
TiII	0.35 ± 0.11	-0.03 ± 0.15	-0.21 ± 0.13	-	0.52 ± 0.13	-	-	0.34 ± 0.10
	0.22 ± 0.15	0.00 ± 0.20	0.24 ± 0.17	0.46 ± 0.22	0.30 ± 0.15	-0.05 ± 0.06	0.04 ± 0.06	0.15 ± 0.10
V	0.54 ± 0.13	0.27 ± 0.18	-0.78 ± 0.15	-	-0.06 ± 0.13	0.08 ± 0.04	0.27 ± 0.04	0.02 ± 0.07
	0.33 ± 0.20	0.3 ± 0.3	-0.54 ± 0.23	-1.24 ± 0.32	-0.50 ± 0.19	-0.13 ± 0.05	-0.14 ± 0.05	-0.14 ± 0.10
Cr	-0.17 ± 0.10	0.05 ± 0.14	0.12 ± 0.12	-0.43 ± 0.15	-0.72 ± 0.10	-0.14 ± 0.03	0.09 ± 0.03	0.04 ± 0.06
	0.00 ± 0.14	-0.03 ± 0.18	0.08 ± 0.16	-0.53 ± 0.21	-0.56 ± 0.13	0.03 ± 0.03	0.06 ± 0.03	-0.07 ± 0.06
Mn	-0.28 ± 0.05	-0.78 ± 0.07	-0.30 ± 0.07	-0.06 ± 0.08	-0.12 ± 0.05	-	-	-0.01 ± 0.03
	-0.45 ± 0.04	-0.77 ± 0.05	-0.41 ± 0.05	-0.28 ± 0.06	-0.24 ± 0.05	0.223 ± 0.016	0.148 ± 0.016	-0.09 ± 0.03
Co	-0.83 ± 0.11	-0.35 ± 0.15	-0.17 ± 0.13	-0.38 ± 0.18	0.12 ± 0.11	0.22 ± 0.03	0.16 ± 0.03	0.19 ± 0.05
	-0.94 ± 0.16	0.05 ± 0.26	-0.09 ± 0.20	0.9 ± 0.3	0.10 ± 0.17	0.27 ± 0.04	0.14 ± 0.04	0.15 ± 0.08
Ni	0.00 ± 0.04	-0.10 ± 0.05	0.05 ± 0.05	-0.26 ± 0.06	0.08 ± 0.04	0.013 ± 0.013	0.142 ± 0.014	0.111 ± 0.024
	-0.05 ± 0.03	-0.15 ± 0.05	0.04 ± 0.04	-0.20 ± 0.05	0.09 ± 0.04	0.011 ± 0.015	0.096 ± 0.015	0.070 ± 0.024
Cu	0.48 ± 0.11	-1.13 ± 0.14	0.25 ± 0.13	0.77 ± 0.16	0.30 ± 0.10	-	-	0.21 ± 0.05
	0.12 ± 0.10	0.24 ± 0.13	-0.25 ± 0.11	0.30 ± 0.15	-	-	-	-
Ce	-0.10 ± 0.11	-0.38 ± 0.16	-0.58 ± 0.12	-0.07 ± 0.18	-0.27 ± 0.11	-0.20 ± 0.06	-0.19 ± 0.06	-0.33 ± 0.08

Table 4. Abundance ratios [X/Fe] for each star from APOGEE ASPCAP DR17. For each element, the first line is the result adopted as calibrated by the APOGEE project, whereas the second line, in bold face, corresponds to the spectroscopic ASPCAP abundance.

puted synthetic spectrum because of the unidentified lines on both sides of the Si I line.

Calcium: Among the five Ca I lines considered in the H -band, only Ca I 16155.235 Å is sufficiently sensitive to Ca abundance. Therefore, we conclude that the Ca abundances from the optical are more reliable than those from the H -band. Figure 3 shows the Ca I lines in the optical for star NGC6558-1160. In this figure, the two very weak lines, Ca I 6464.679 and 6508.840 Å, are not useful in this metal-poor star but they are useful in metal-rich stars.

The odd-Z elements Na and Al: As discussed in Barbay et al. (2023), the Na lines in the H -band are not reliable. As the lines in the optical are reliable, this band should be favoured for this element. Al I 16718.957, 16750.539 and 16763.358 Å are very suitable lines, whereas, in the optical, the Al I 6696 and 6698 Å are strong in the field metal-rich stars, but rather weak in the metal-poor stars. Table 7 reports the abundances derived from atomic lines of Mg I, Al I, Si I, and Ca I in the H -band computed with TURBOSPECTRUM based on the lines reported in Table 1. Table 8 reports the abundances derived from atomic lines of Na I, Mg I, Al I, Si I, Ca I, Ti I, and Ti II in the optical, which are computed with TURBOSPECTRUM based on the lines reported in, for example, Barbay et al. (2016).

5. Discussion

In this work, we fitted the lines in the optical and H -band and compared the results between these two sets. If the resulting abundances of some lines needed for the fits are too overabundant or too deficient, this indicates that the stellar parameters are not suitable.

5.1. Stellar parameters

Adopting the stellar parameters from the optical, the stars NGC6558-283 and NGC6558-1160 show weaker OH lines than observed, even considering a high oxygen abundance of [O/Fe]=0.5 - 0.6 (Table 6), indicating that the effective temperature is probably too hot, and therefore that the ASPCAP parameters, which give considerably lower effective temperatures, are more suitable. The same applies to star Pal6-401, but with less discrepant effective temperatures between ASPCAP and optical.

The excessively high temperature derived from the optical is probably due to difficulties in measuring Fe lines because of blends, continuum placement, and noise. In conclusion, for the two stars in NGC 6558, the APOGEE stellar parameters, as well

Element	HP1-2	283	1160	402361	401	545277	82760	392918
UVES								
C	0.00±0.15	0.15±0.11	0.20±0.11	0.00±0.15	-0.12±0.15	-0.10±0.07	0.00±0.07	0.08±0.07
N	0.50±0.15	0.80±0.11	1.00±0.11	—	0.82±0.08	0.00±0.16	0.05±0.16	0.40±0.16
O	0.30±0.15	0.40±0.11	0.50±0.11	0.50±0.12	0.45±0.15	-0.10±0.08	-0.10±0.08	0.20±0.08
Na	-0.02±0.05	0.15±0.11	0.00±0.11	-0.22±0.05	0.10±0.15	—	—	—
Mg	0.15±0.06	—	0.40±0.11	0.33±0.05	0.30±0.17	—	—	—
Al	-0.28±0.12	0.30±0.12	0.00±0.12	-0.30±0.12	0.40±0.17	—	—	—
Si	0.30±0.14	—	0.20±0.10	0.17±0.10	0.41±0.17	—	—	—
Ca	-0.04±0.15	0.00±0.13	0.16±0.13	0.16±0.05	0.34±0.18	—	—	—
TiI	0.07±0.13	0.15±0.15	0.15±0.15	0.03±0.10	0.32±0.18	—	—	—
TiII	0.10±0.15	0.20±0.14	0.27±0.14	0.17±0.10	—	—	—	—
Sc	-0.05±0.07	-0.16±0.16	-0.13±0.16	-0.11±0.12	—	—	—	—
V	-0.22±0.09	-0.01±0.03	-0.01±0.03	-0.06±0.06	—	—	—	—
Mn	-0.57±0.05	-0.45±0.05	-0.45±0.05	-0.55±0.05	—	0.00±0.05	0.00±0.05	0.00±0.05
Co	—	—	—	—	—	-0.13±0.09	-0.02±0.09	0.00±0.09
Cu	-1.0±0.15	-0.50±0.16	-0.70±0.16	-0.45±0.12	—	-0.30±0.12	-0.35±0.12	-0.50±0.12
Zn	0.30±0.15	-0.10±0.15	0.20±0.15	0.1±0.05	—	0.00±0.05	-0.30±0.05	0.15±0.05
Y	-0.15±0.15	0.75±0.19	0.56±0.19	0.32±0.25	0.09±0.15	—	—	—
Zr	—	—	—	0.20±0.20	0.41±0.35	—	—	—
Ba	0.65±0.16	0.00±0.10	0.15±0.10	0.45±0.23	0.49±0.13	0.16±0.21	0.36±0.21	0.06±0.21
La	-0.15±0.12	—	—	0.20±0.16	0.24±0.16	—	0.16±0.11	0.16±0.11
Ce	—	—	—	—	—	0.04±0.11	-0.34±0.11	0.08±0.11
Nd	—	—	—	—	—	-0.46±0.08	-0.22±0.08	-0.08±0.08
Eu	0.40±0.15	0.80±0.12	0.30±0.12	0.40±0.12	0.58±0.11	0.26±0.10	-0.20±0.10	0.26±0.10

Table 5. Abundance ratios $[X/Fe]$ obtained from UVES optical spectra for sample stars from Barbuy et al. (2013, 2014, 2015, 2016, 2018a), Ernandes et al. (2018, 2020); Friaça & Barbuy (2017); Lecureur et al. (2007); Souza et al. (2021); van der Swaelmen et al. (2016). Abundances in bold face were computed in the present work.

Model Star	Turbospectrum H -band																
	APO UVES HP1-2		APO UVES 283		APO UVES DGD 1160			APO UVES 402361		APO UVES 401		APO UVES 545277		APO UVES 82760		APO UVES 392918	
C	-0.15	-0.15	0.12	0.35	0.00	0.00	0.15	0.08	0.08:	0.00	0.45	0.00	+0.10	-0.30	-0.10	-0.15	-0.20
N	0.60	0.40	0.35	0.80	0.00	0.10	0.10	0.30	0.30:	0.20	0.2	0.00	+0.40	0.30	+0.05	0.15	0.10
O	0.27	0.45	0.45	0.50:	0.30	0.30	0.40	0.42	0.50:	0.25	0.50:	0.00	+0.50	0.30	-0.05	0.20	0.10

Table 6. C, N, and O abundances from TURBOSPECTRUM calculations of APOGEE spectra for both sets (optical and H -band) of stellar parameters.

Model Star	Turbospectrum															
	APO UVES HP1-2		APO UVES 283		APO UVES 1160		APO UVES 402361		APO UVES 401		APO UVES 545277		APO UVES 82760		APO UVES 392918	
Mg	0.30	0.20	0.20	0.32	0.25	0.40	—	0.30	0.28	0.20	0.00	0.00	0.00	-0.15	0.10	0.10
Al	0.40	0.23	0.75	0.90	0.00	0.40	—	—	0.08	0.35	0.30	0.65	0.70	0.50	0.70	0.35
Si	0.50	0.20	0.40	0.30	0.20	0.40	0.30	0.30	0.42	0.45	0.00	0.06	0.15	0.05	0.35	0.15
Ca	0.20	-0.05	—	—	0.20	0.50	0.20	0.25	0.22	0.30	0.40	0.35	0.50	0.05	0.40	0.15
Ti	—	—	—	—	—	—	...	—	—	—	—	—	—	—	—	—

Table 7. TURBOSPECTRUM calculations of APOGEE spectra based on both APOGEE and UVES stellar parameters.

as the parameters from González-Díaz et al. (2023), are more suitable.

For the star OGLE-545277, the ASPCAP parameters show a very high metallicity of $[Fe/H]=+0.54$, which is probably an overestimate, and this leads to a low oxygen abundance of $[O/Fe]=-0.35$; the optical parameters give a reasonable metallicity of $[Fe/H]=+0.07$.

For OGLE-82760, despite very similar parameters, the low microturbulence velocity from ASPCAP requires a somewhat

lower O abundance. The abundances required to fit the lines Mg, Si, Ca, and Ti are far too strong ($[X/Fe]>0.40$) for the fits of three OGLE stars (OGLE-545277, OGLE-82760, and OGLE-392918) using the ASPCAP stellar parameters, which is not expected for solar-metallicity stars. Therefore, the optical parameters given in Zoccali et al. (2006) and Lecureur et al. (2007) are clearly more suitable than the ASPCAP parameters for these three solar-metallicity stars. The stars HP1-2, NGC 6522-402361, and, to a lesser extent, Palomar6-401 have similar

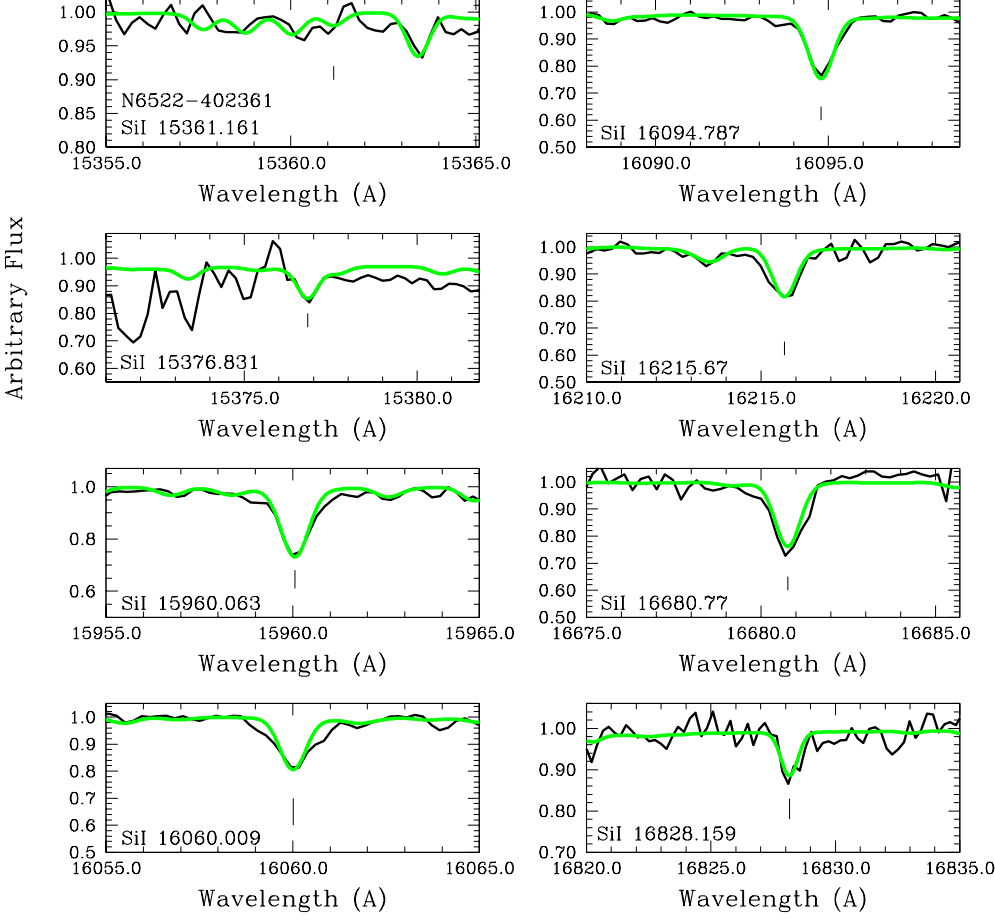


Fig. 2. *H*-band Si I lines shown for the star NGC6522-402361. The APOGEE observed spectrum (black line) is compared with synthetic spectra computed adopting the UVES stellar parameters and $[\text{Si}/\text{Fe}]=+0.30$ (green lines).

Model Star	Turbospectrum															
	APO UVES HP1-2		APO UVES 283		APO UVES 1160		APO UVES 402361		APO UVES 401		APO UVES 545277		APO UVES 82760		APO UVES 392918	
Na	0.50	0.20	0.50	0.30	0.25	0.45	0.05	0.10	-0.20	0.00	0.90	0.80	0.7	0.40	0.60	0.35
Mg	0.30	0.20	0.20	0.20	0.25	0.40	0.30	0.30	0.23	0.21	—	0.00	0.00	-0.15	0.20:	0.10:
Al	0.45	0.30	0.60	0.35	—	—	0.30	0.35	0.15	0.35	0.80	0.65	0.50	0.50	0.80	0.35
Si	0.40	0.20	0.45	0.35	0.40	0.40	0.10	-0.10	0.40	0.45	0.00	0.00	0.20	0.05	0.35	0.15
Ca	0.25	-0.05	0.15	0.25	0.25	0.35	-0.15	0.00	0.0:	0.0:	0.55	0.40	0.40	0.05	>0.8	0.15
Ti	0.30	0.15	0.20	0.45	0.15	>0.40	0.25	0.25	0.10	0.20	>0.5	0.40	>0.50	0.30	≥0.70	0.0

Table 8. TURBOSPECTRUM calculations of lines in the UVES optical spectra based on both APOGEE and UVES stellar parameters.

Model Star	<i>H</i> -band HP1-2		<i>H</i> -band 283		<i>H</i> -band 1160		<i>H</i> -band 402361		<i>H</i> -band 401		<i>H</i> -band 545277		<i>H</i> -band 82760		<i>H</i> -band 392918	
	Opt	Opt	Opt	Opt	Opt	Opt	Opt	Opt	Opt	Opt	Opt	Opt	Opt	Opt	Opt	
C	-0.15	—	0.12	—	0.00	—	0.08	—	0.00	—	0.10	—	-0.10	—	-0.20	—
N	0.40	—	0.35	—	0.00	—	0.30	—	0.20	—	0.40	—	0.05	—	0.10	—
O	0.45	—	0.45	—	0.30	—	0.50	—	0.25	—	0.50	—	-0.05	—	+0.10	—
Na	—	-0.20	—	0.50	—	0.25	—	0.08	0.03	-0.10	0.70	0.80	0.37	0.40	0.00	0.35
Mg	0.21	0.15	0.24	—	0.25	0.25	0.30	0.30	0.24	0.23	0.00	0.00	-0.15	-0.15	0.10	0.10
Al	0.32	0.37	0.90	0.60	0.40	—	0.08	0.32	0.32	0.25	0.70	0.65	0.70	0.50	0.35	0.35
Si	0.35	0.30	0.40	0.45	0.20	0.40	0.30	0.00	0.30	0.46	0.06	0.00	0.05	0.05	0.15	0.15
Ca	0.12	0.10	—	0.15	0.20	0.25	0.22	-0.07	0.26	0.00	0.35	0.48	0.05	0.05	0.15	0.15
Ti	—	0.22	—	0.20	—	0.15	—	0.25	—	0.15	—	0.40	—	0.30	—	0.00

Table 9. Abundances derived from APOGEE and UVES spectra with TURBOSPECTRUM, adopting the best-suited stellar parameters, as explained in Sect. 4.1.

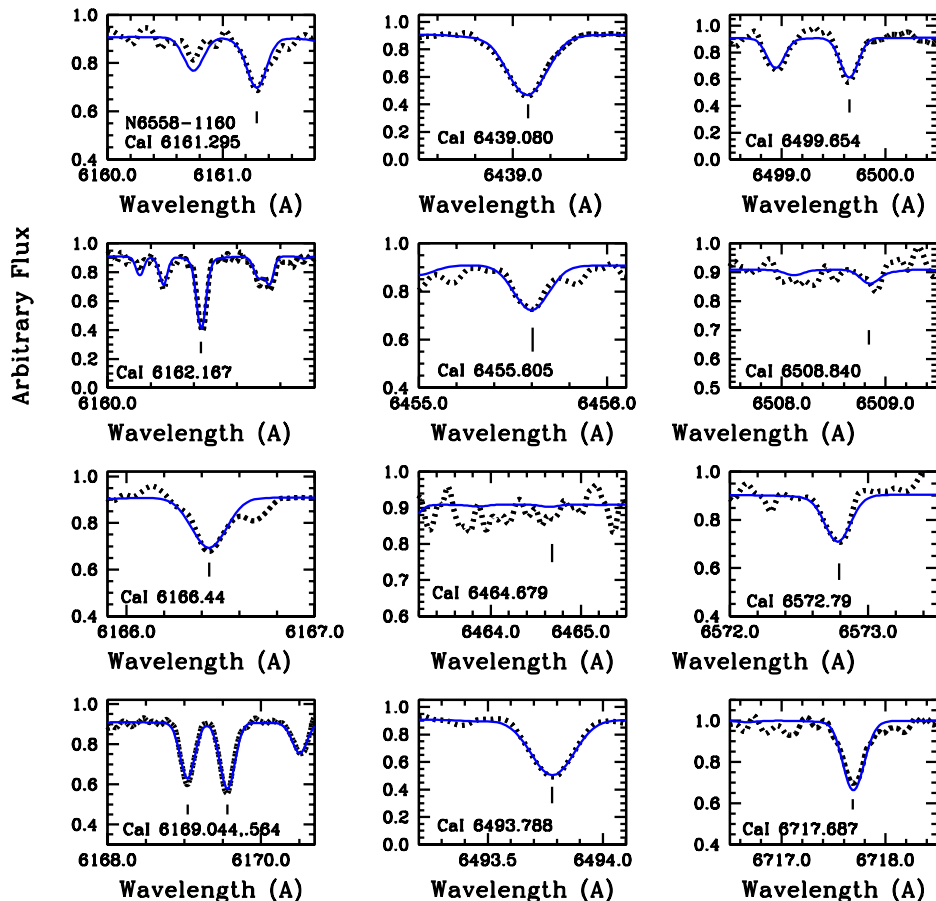


Fig. 3. Optical Ca I lines shown for the star NGC6558-1160. The UVES observed spectrum (black line) is compared with synthetic spectra computed adopting the UVES and APOGEE stellar parameters, with $[\text{Ca}/\text{Fe}]=0.15$ and 0.25 for UVES and APOGEE stellar parameters, respectively (blue and green lines are coincident).

parameters derived from the optical and H -band, and they appear suitable.

5.2. Discussion on atomic lines in the H -band and optical

Mg I, Al I, and Si I lines are suitable in the H -band and optical. The listed lines may be limited for more metal-poor stars in the case of Mg and Si, and of Al in the optical. Si has better (stronger) lines in the H -band, whereas the lines are rather weak in the optical.

Ca I lines considered in the H -band are not fully suitable because of blends. The lines in the optical are more suitable.

As discussed in Razera et al. (2022) and Barbuy et al. (2023), Na I, and Ti I in the H -band, are too blended—or too weak in the case of Na. For these two elements, the optical is better suited.

Following these conclusions, and adopting the more suitable stellar parameters, the final abundances are given in Table 9. This table shows the remarkable agreement between abundances, within errors, derived from H -band and optical, once the correct stellar parameters are chosen.

5.3. Comparison with bulge data

The sample is compared with the bulge field stars from the reduced proper motion (RPM) sample by Queiroz et al. (2021, hereafter Q21). Figures 4 and 5 show our sample over-plotted on the Q21 sample. Our data are a good fit to the large sample by

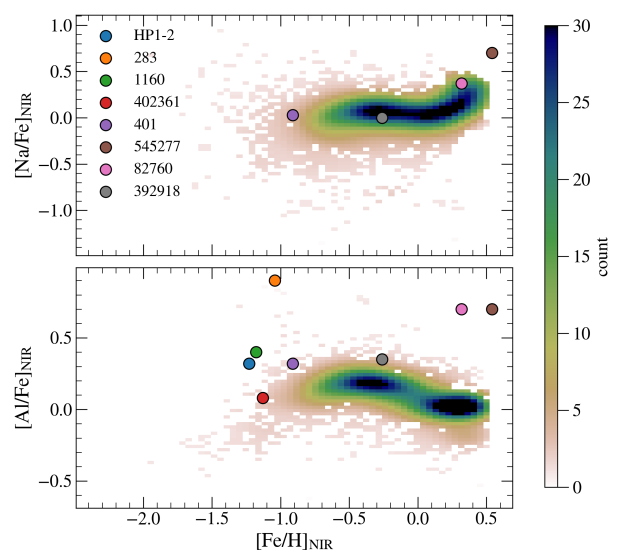


Fig. 4. $[\text{Na}/\text{Fe}]$ and $[\text{Al}/\text{Fe}]$ vs. $[\text{Fe}/\text{H}]$ for the final results given in Table 9, using the H -band spectra, over-plotted on the bulge sample by Queiroz et al. (2021).

Q21, and we can say that, although our sample is small, it does represent the behaviour of bulge stars for the alpha elements and the odd- Z elements Na and Al.

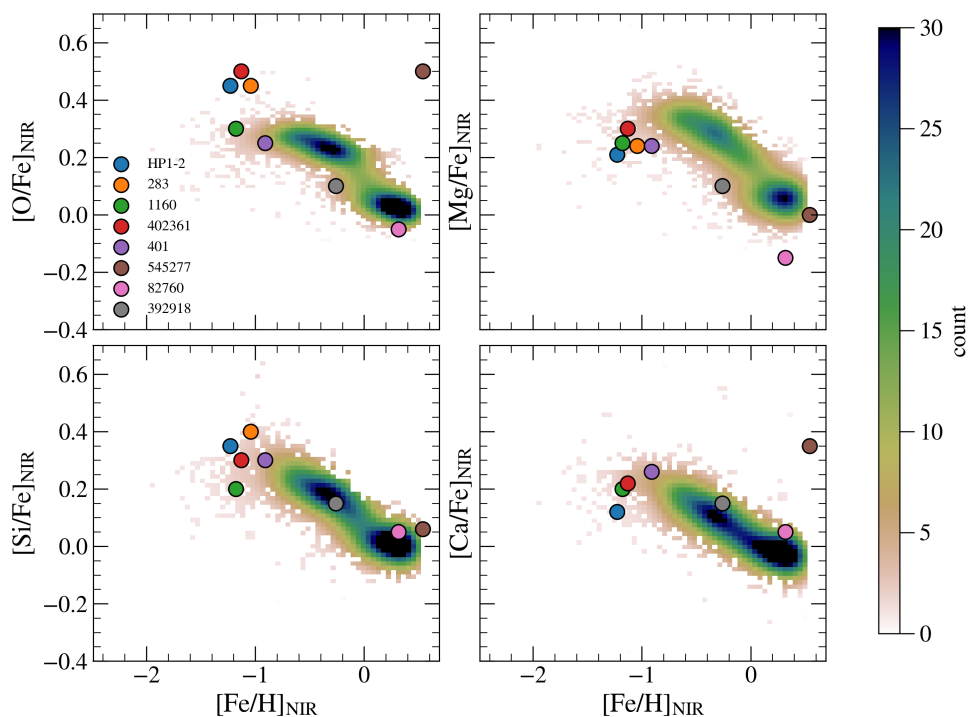


Fig. 5. Same as Fig. 4 but for $[\alpha\text{-elements}/\text{Fe}]$ vs. $[\text{Fe}/\text{H}]$.

5.4. Errors

The line-fitting procedure, given the high resolution of the spectra, has an error of $\sim \pm 0.1$ for all lines. The error in abundances depends for the most part on the stellar parameters, with the presence of blends being a secondary source of errors, as discussed for some of the lines (e.g., for Ca I lines in the H -band).

Figure 6 gives the abundance differences between the derivation in the H -band and optical based on the final stellar parameters (Table 9), both as a function of atomic number Z and per star vs. $[\text{Fe}/\text{H}]$. The larger differences are for Al (± 0.3) and the smallest for Mg. These results show the good agreement between the derivation of abundances from the H -band and optical, as long as suitable stellar parameters are adopted.

6. Conclusions

In this work, we compared abundance results obtained from optical spectra (VLT/UVES) and H -band spectra (APOGEE) for eight bulge stars. The calculations were carried out adopting stellar parameters from the literature obtained from optical and H -band spectra. We then computed abundances employing the TURBOSPECTRUM code throughout for the sake of homogeneity, adopting the two sets of stellar parameters for the lines in the optical and the H -band. The aim of this work is to find the best methods for deriving stellar parameters and their advantages and disadvantages, and to identify the best lines for each of the analyzed elements.

A first and important conclusion is that the stellar parameters—and in particular the effective temperatures obtained from ASPCAP—that correspond to a spectroscopic solution minimizing the chi-squared differences between the observations and the models in seven dimensions, lead to reliable parameters. This is due to the derivation of C, N, and O abundances through the strength of molecular lines of CO, CN, and OH, leading to reliable effective temperature, and more so when dealing with high-S/N spectra. This is an important compensation for the lack of

Fe I lines of varied excitation energies, which are used to constrain effective temperatures in the optical.

In conclusion, as concerns stellar parameters, previous APOGEE and UVES results are suitable for stars HP1-2, NGC6522-402361 and Palomar6-401. A too high effective temperature was estimated for the stars N6558-283 and NGC6558-1160 from the optical, therefore the ASPCAP parameters are more suitable. For the 3 metal-rich stars the optical parameters derived are more suitable than the ASPCAP ones.

Regarding the atomic lines, the Mg, Al, and Si lines in both H -band and optical are suitable, with Si having stronger lines in the H -band than in the optical. For Ca, the optical appears to have a greater number of reliable lines. Na and Ti do not have reliable lines in the H -band, and therefore the optical lines are more suitable.

This findings of study will be particularly useful for future observations with the ELT/MOSAIC spectrograph, which will allow simultaneous observations of the H -band and selected regions in the optical.

Finally, a comparison of abundances in the presently studied 8 stars with bulge field stars by Queiroz et al. (2021) shows good agreement, and despite the limited number of stars in our sample, they cover the entire bulge metallicity range.

Acknowledgements

PS acknowledges Fundação de Amparo à Pesquisa do Estado de São Paulo (FAPESP) post-doctoral fellowships 2020/13239-5 and 2022/14382-1. BB acknowledges grants from FAPESP, Conselho Nacional de Desenvolvimento Científico e Tecnológico (CNPq) and Coordenação de Aperfeiçoamento de Pessoal de Nível Superior (CAPES) - Financial code 001. SOS acknowledges a FAPESP PhD fellowship no. 2018/22044-3. PS, BB, HE, and SOS are part of the Brazilian Participation Group (BPG) in the Sloan Digital Sky Survey (SDSS), from the Laboratório Interinstitucional de e-Astronomia – LIneA, Brazil. J.G.F-T gratefully acknowledges the grant support provided by

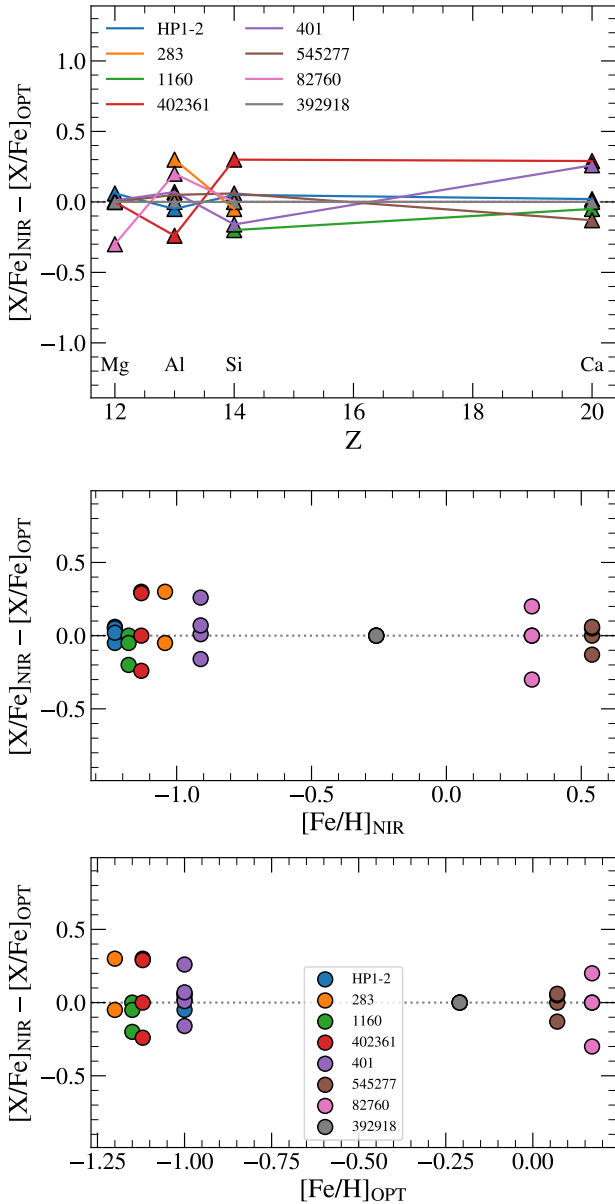


Fig. 6. Abundance difference between H -band and optical (Table 9) as a function of atomic number Z , and per star vs. $[Fe/H]$.

Proyecto Fondecyt Iniciación No. 11220340, Proyecto Fondecyt Postdoc No. 3230001 (Sponsored by J.G.F-T) and from the Joint Committee ESO-Government of Chile 2021 (ORP 023/2021), and 2023 (ORP 062/2023). D.G-D gratefully acknowledges support from the Joint Committee ESO-Government of Chile 2021 (ORP 023/2021), as well as the support from call N° 785 of 2017 of the Colombian Departamento Administrativo de Ciencia, Tecnología e Innovación (COLCIENCIAS). Apogee project: Funding for the Sloan Digital Sky Survey IV has been provided by the Alfred P. Sloan Foundation, the U.S. Department of Energy Office of Science, and the Participating Institutions. SDSS acknowledges support and resources from the Center for High-Performance Computing at the University of Utah. The SDSS web site is www.sdss.org. SDSS is managed by the Astrophysical Research Consortium for the Participating Institutions of the SDSS Collaboration including the Brazilian Participation Group, the Carnegie Institution for Science, Carnegie Mellon

University, Center for Astrophysics | Harvard & Smithsonian (CfA), the Chilean Participation Group, the French Participation Group, Instituto de Astrofísica de Canarias, The Johns Hopkins University, Kavli Institute for the Physics and Mathematics of the Universe (IPMU) / University of Tokyo, the Korean Participation Group, Lawrence Berkeley National Laboratory, Leibniz Institut für Astrophysik Potsdam (AIP), Max-Planck-Institut für Astronomie (MPIA Heidelberg), Max-Planck-Institut für Astrophysik (MPA Garching), Max-Planck-Institut für Extraterrestrische Physik (MPE), National Astronomical Observatories of China, New Mexico State University, New York University, University of Notre Dame, Observatório Nacional / MCTI, The Ohio State University, Pennsylvania State University, Shanghai Astronomical Observatory, United Kingdom Participation Group, Universidad Nacional Autónoma de México, University of Arizona, University of Colorado Boulder, University of Oxford, University of Portsmouth, University of Utah, University of Virginia, University of Washington, University of Wisconsin, Vanderbilt University, and Yale University.

Data Availability

The spectra observed in the optical with the UVES spectrograph are available at the archival data from the European Southern Observatory (ESO). The spectra observed in the H -band are from the APOGEE survey.

References

- Alvarez, R., Plez, B. 1998, *A&A*, 330, 1109
 Barbuy, B., Zoccali, M., Ortolani, S., et al. 2009, *A&A*, 507, 405
 Barbuy, B., Hill, V., Zoccali, M., et al. 2013, *A&A*, 559, 5
 Barbuy, B., Chiappini, C., Cantelli, E., et al. 2014, *A&A*, 570, 76
 Barbuy, B., Friaça, A. C. S., da Silveira, C. R., et al. 2015, 580, 40
 Barbuy, B., Cantelli, E., Vemado, A., et al. 2016, *A&A*, 591, 53
 Barbuy, B., Chiappini, C., Gerhard, O. 2018a, *ARA&A*, 56, 223
 Barbuy, B., Trevisan, J., & de Almeida, A. 2018b, *PASA*, 35, 46
 Barbuy, B., Muniz, L., Ortolani, S., et al. 2018, *A&A*, 619, 178
 Barbuy, B., Cantelli, E., Muniz, L., et al. 2021, *A&A*, 654, 29
 Barbuy, B., Friaça, A. C. S.; Ernandes, H., et al. 2023, *MNRAS*, 526, 2365
 Bastian, N., Lardo, C. 2018, *ARA&A*, 56, 83
 Beaton, R. L., Oelkers, R.J., Hayes, C. R., et al. 2021, *AJ*, 162, 302
 Blanton, M. R., et al. 2017, *AJ*, 154, 28
 Brooke, J. S. A., Bernath, P. F., Schmidt, T. W., et al. 2013, *JQSR*, 124, 11
 Brooke, J. S. A., Ram, R. S., Western, C. M., et al. 2014, *ApJS*, 210, 23
 Cunha, K., Smith, V. V., Hasselquist, S., et al. 2017, *ApJ*, 844, 145
 da Silveira, C. R. Barbuy, B., Friaça, A.C.S., et al. 2018, *A&A*, 614, A149
 Ernandes, H., Barbuy, B., Alves-Brito, A., et al. 2018, *A&A*, 616, 18
 Ernandes, H., Barbuy, B., Friaça, A. C. S., et al. 2020, *A&A*, 640, 89
 Fernández-Trincado, J. G., Robin, A. C., Moreno, E., et al. 2016, *ApJ*, 833, 132
 Friaça, A. C. S., & Barbuy, B. 2017, *A&A*, 598, A121
 García-Pérez, A. E., Allende Prieto, C., Holtzman, J. A., et al. 2016, *AJ*, 151, 144
 González-Díaz, D., Fernández-Trincado, J.G., Villanova, S., et al. 2023, *MNRAS*, submitted
 Grevesse, N., Sauval, A. J. 1998, *SSRv*, 85, 161
 Gunn J. E., et al., 2006, *AJ*, 131, 2332
 Gustafsson, B., Edvardsson, B., Eriksson, K., et al. 2008, *A&A*, 486, 951
 Hammer, F., Morris, S., Cuby, J.-G., et al. 2021, *The Messenger*, 182, 33
 Hawkins, K., Masseron, T., Jofré, P., et al. 2016, *A&A*, 594, A43
 Hayes, C.R., Masseron, T., Sobeck, J., et al. 2022, *ApJS*, 262, 34
 Holtzman, J. A., Hasselquist, S., Shetrone, M., et al. 2018, *AJ*, 156, 125
 Hubeny, I., Lanz, T. 2017, [arXiv1706.01859H](https://arxiv.org/abs/1706.01859)
 Hubeny, I., Allende Prieto, C., Osorio, Y., Lanz, T. 2021, [arXiv2104.02829](https://arxiv.org/abs/2104.02829)
 Jönsson, H., Ryde, N., Schultheis, M., Zoccali, M. 2017, *A&A*, 598, A101
 Jönsson, H., Allende Prieto, C., Holtzman, J. A., et al. 2018, *ApJ*, 156, 126
 Jönsson, H., Holtzman, J. A., Allende Prieto, C. A., et al. 2020, *AJ*, 160, 120
 Jorgensen, U. G. 1994, *A&A*, 284, 179
 Lecureur, A., Hill, V., Zoccali, M., et al. 2007, *A&A*, 465, 799
 Majewski, S. R., Schiavon, R. P., Frinchaboy, P. M., et al. 2017, *AJ*, 154, 94
 Masseron, T., Plez, B., van Eck, S. et al. 2014, *A&A*, 571, A47
 Matteucci F. 2021, *A&ARv*, 29, 5

- Milone, A.P., Piotto, G., Renzini, A., et al. 2017, *MNRAS*, 464, 3636
- Milone, A.P., Marino, A.F. 2022, *Univ*, 8, 359
- Minniti, D., Matsunaga, N., Fernández-Trincado, J. G., et al. 2024, 2023Arxiv2312.16028
- Nelder, J.A., Mead, R. 1965, *CompJ*, 7, 308
- Osorio, Y., Allende Prieto, C., Hubeny, I., Mészáros, Sz., Shetrone, M. 2020, *A&A*, 637, A80
- Piotto, G., Milone, A. P., Bedin, L. R., et al. 2015, *AJ*, 149, 91
- Plez, B. 2012, *ASCL*, ascl:1205.004
- Queiroz, A. B. A., Chiappini, C., Pérez-Villegas, A., et al. 2021, *A&A*, 656, A156
- Razera, R., Barbuy, B., Moura, T. C., et al. 2022, *MNRAS*, 517, 4590
- Renzini, A., D'Antona, F., Cassisi, S., et al. 2015, *MNRAS*, 454, 4197
- Ryabchikova, T., Piskunov, N., Kurucz, R. L., et al. 2015, *PhyS*, 90, 054005
- Santana, F. A., Beaton, R. L., Covey, K. R., et al. 2021, *AJ*, 162, 303
- Skory, S., Weck, P. F., Stancil, P. C., et al. 2003, *ApJS*, 148, 599
- Smith, V., Cunha, K., Shetrone, M. D., et al. 2013, *ApJ*, 765, 16
- Smith, V., Bizyaev, D., Cunha, K., et al. 2021, *AJ*, 161, 254
- Souto, D., Cunha, K., Smith, V., et al. 2016, *ApJ*, 830, 35
- Souza, S. O., Valentini, M., Barbuy, B., et al. 2021, *A&A*, 656, 78
- Steffen, M., Prakashavičius, D., Caffau, E., et al. 2015, *A&A*, 583, 57
- van der Swaelmen, M., Barbuy, B., Hill, V., et al. 2016, *A&A*, 586, A1
- Wilson, J.C., et al. 2019, *PASP*, 131, 50001
- Zasowski, G., et al. 2013, *AJ*, 146, 81
- Zasowski, G., et al. 2017, *AJ*, 154, 198
- Zasowski, g., Schultheis, M., Hesselquist, S., et al. 2019, *ApJ*, 870, 138
- Zoccali, M., Lecureur, A., Barbuy, B., et al. 2006, *A&A*, 457, L1
- Zoccali, M., Hill, V., Lecureur, A., et al. 2008, *A&A*, 486, 177